1   **Local opposite orientation preferences in V1: fMRI sensitivity to fine-grained**
2   **pattern information**

3   Corresponding author: arjen.alink@mrc-cbu.cam.ac.uk

1

Local opposite orientation preferences in V1: fMRI sensitivity to fine-grained pattern information

Arjen Alink[1], Alexander Walther[1], Alexandra Krugliak[2] & Nikolaus Kriegeskorte[1]

[1]MRC Cognition and Brain Sciences Unit, Cambridge UK   [2]University of Birmingham, UK

The orientation of a visual grating can be decoded from human primary visual cortex (V1) using functional magnetic resonance imaging (fMRI) at conventional resolutions (2-3 mm voxel width, 3T scanner). It is unclear to what extent this information originates from different spatial scales of neuronal selectivity, ranging from orientation columns to global areal maps. According to the global-areal-map account, fMRI orientation decoding relies exclusively on fMRI voxels in V1 exhibiting a radial or vertical preference. Here we show, by contrast, that 2-mm isotropic voxels in a small patch of V1 within a quarterfield representation exhibit reliable opposite selectivities. Sets of voxels with opposite selectivities are locally intermingled and each set can support orientation decoding. This indicates that global areal maps cannot fully account for orientation information in fMRI and demonstrates that fMRI also reflects fine-grained patterns of neuronal selectivity.

Significance statement Conventional (3T) f*unctional magnetic resonance imaging (fMRI) allows one measure brain activity at a spatial resolution of 2-3 mm. Brain response patterns in the primary visual cortex (V1) measured with fMRI have been shown to contain robust information about the orientation of visual grating stimuli. However, it is unclear whether this information arises only from global-areal patterns or also from more fine-grained patterns. Here we show that opposite orientation preferences are present and replicable within small V1 patches. This finding demonstrates that fine-grained fMRI patterns contribute to the orientation information present in fMRI data.*

Visual orientation is known to be represented in columnar preference patterns in the primary visual cortex (V1) at a sub-millimetre scale (Yacoub et al., 2008). Kamitani and Tong (2005) demonstrated that fMRI patterns measured in V1 at standard resolution (3-mm isotropic voxels) provide information about the orientation of visual gratings. This study had a big impact in part because it suggested a sensitivity of standard-resolution fMRI to columnar-scale neuronal selectivity patterns. However, it has been proposed that V1 orientation decoding might rely on coarse-scale organisations instead (Op de Beeck et al. 2010). In particular, several studies demonstrated slight preferences for radial orientations (Sasaki et al., 2006; Mannion et al., 2010; Freeman et al. 2011; Alink et al., 2013), which might explain orientation decoding results. A left-tilted diagonal grating, for example, will have approximately radial orientation in the upper left and lower right quadrants, driving the corresponding quarterfield representations of V1 more strongly than the other two quarterfield representations (Sasaki et al., 2006). It has been argued that this effect completely explains fMRI orientation decoding (Freeman et al. 2011).

One way to minimize a contribution to orientation decoding from the radial-preference map is to use logarithmic spiral stimuli. A logarithmic spiral has a constant orientation relative to the radial direction, e.g. 45°. Two spirals with orientations 45° and -45°, respectively, relative to the radius are orthogonal to each other everywhere. They are also balanced about the radial direction everywhere, and thus radial preference cannot account for their decodability. However, such spirals have been shown to be robustly decodable (Mannion et al. 2010; Alink et al., 2013; Freeman et al., 2013). In addition to radial-preference, however, there is evidence that V1 patches also respond preferentially to vertical orientation (Mannion et al., 2010; Alink et al. 2013; Freeman et al., 2013). This global vertical preference predicts distinct global-areal patterns to be elicited by opposite-sense spirals and, thus, spiral decoding as well might be explained by global-areal-scale pattern information.

The aim of the current study is to test if fMRI response patterns with a grain finer than these two coarse-scale preference maps contribute to orientation decoding. The observation that orientation

51 decodability is robust to high-pass filtering of fMRI patterns has been considered as evidence for a
52 fine-grained contribution to fMRI orientation decoding (Swisher et al., 2010; Shmuel et al., 2010;
53 Alink et al., 2013). Filtering analysis, however, is not able to conclusively determine whether fine-
54 grained activation patterns contribute to orientation decoding because coarse-scale neural effects
55 can give rise to spurious high-spatial frequency fMRI pattern information if adjacent voxels have
56 different sensitivity to local neural activity. This effect is illustrated in Figure 1. Differences in
57 sensitivity (the voxel gain field) can result, for example, from partial volume sampling, with some
58 voxels sampling mainly gray matter and others mainly white matter. A voxel gain field is not
59 expected to invert the sign of a contrast between two stimuli. Therefore, if orientation decoding of
60 gratings and spirals originated solely from coarse-scale radial and vertical preferences, respectively,
61 then one would not expect voxels in a local cluster to exhibit reliable opposite preferences. Under
62 the global areal account of grating decoding (i.e. radial preference), a small patch of V1 representing
63 a region within one visual quarterfield should not contain voxels preferring tangential over radial
64 stimuli. Similarly, under the global areal account of spiral decoding (i.e. vertical preference), a small
65 patch of V1 representing a region within one visual quarterfield should not contain voxels preferring
66 horizontal over vertical stimuli. Here we show that local voxel clusters in V1 do exhibit reliable
67 preferences for both radial and tangential orientations (in the gratings scenario) and for both vertical
68 and horizontal orientations (in the spirals scenario). The opposite preferences are intermingled
69 within small patches of V1, forming a fine-grained pattern. Gratings can robustly be decoded using
70 either only the radial-preferring or only the tangential-preferring voxels. Similarly, spirals can be
71 decoded using either only the vertical-preferring or only the horizontal-preferring voxels. These
72 results clearly demonstrate the reliable presence of voxels of opposite selectivity within local small
73 patches of V1. Fine-grained fMRI patterns, thus, contribute to orientation decoding.

74 **Materials and methods**

75 **Stimuli and design**

76 *Common features of all stimuli.* All stimulus types were presented within an annulus (inner radius =
77 1.5°, outer radius = 7.04°) centered on fixation on a mid-gray background. The annulus was divided
78 into 36 log-polar tiles defined by twelve radial lines emanating from the center at 30° offsets and
79 two concentric divisions exponentially spaced between the inner and outer radii (radii including
80 inner and outer: 1.50°, 2.51°, 4.20°, 7.04°). This log-polar tiling was apparent in the form of mid-gray
81 "grout lines" present in all stimuli. For each stimulus type there were two exemplars, which had 90°
82 orientation disparity at every location within the annulus. The oriented edges of all stimuli had 100%
83 contrast. The phases of the oriented edges were randomized across presentations of the same
84 exemplar.

85 *Gratings.* The orientation of the gratings was 45° clockwise and 45° anti-clockwise from the vertical.
86 The gratings had a spatial frequency of 1.25 cycles per visual degree. This spatial frequency drives V1
87 strongly (Henriksson et al., 2008) and ensures that even the smallest tiles of the log-polar array
88 contains more than a full spatial cycle.

89 *Spirals.* We used logarithmic spirals whose edges were at a constant angle of +/-45° relative to the
90 radius emanating from fixation. The spiral stimuli had 22 rectangular contrast cycles along the
91 perimeter. This number of cycles along the perimeter was chosen so as to approximately match the
92 spirals' average spatial frequency across radii to that of the uniform gratings. The two spiral
93 exemplars differed in sense: clockwise or anti-clockwise, lending them 90° orientation disparity at
94 every location. Spiral stimuli are radially balanced because clockwise and anti-clockwise spiral stimuli
95 deviate equally (45°), though in opposite directions, from local radial orientations.

96 *Experimental design.* Stimuli were presented to each subject in a single fMRI session comprising
97 eight scanner runs, each of which lasted eight minutes. During each run, we presented both

98   exemplars of one stimulus type (e.g. clockwise and anti-clockwise spirals). Subjects were presented
99   with two runs for each stimulus type. Each run was divided into four equal subruns. Each subrun
100   contained six stimulus blocks (three blocks for each exemplar, with exemplars alternating across
101   blocks and the leading exemplar alternating across subruns). Each block lasted 14 s and contained
102   phase-randomized versions of a single exemplar. During a stimulus block, 28 phase-randomized
103   versions of the exemplar were presented at a frequency of 2 Hz. The stimulus duration was 250 ms,
104   followed by an interstimulus interval (ISI) of 250 ms, during which only the fixation dot and a tiny
105   task-related ring around it was visible (see Task, below).

106   *Retinotopic mapping stimuli.* In order to define regions of interest (ROIs) within V1, we presented
107   dynamic grating stimuli designed to optimally drive early visual cortex. Like the main-experimental
108   stimuli, these stimuli were based on a log-polar array (Figure 2), but without the grout lines and with
109   20 patches per ring. Each patch contained rectangular gratings with a spatial period of one third of
110   the patch's radial width. Grating orientation and phase was assigned randomly to each patch. Over
111   time, the phase of the gratings increased continuously (1 cycle per second) resulting in continuous
112   motion in each patch (in different directions). In addition, the orientation of the grating increased in
113   steps of $\pi/6$, once each second, resulting in motion direction changes within patches over time. We
114   used five such stimuli, driving different parts of the retinotopic representations in V1: (1) a
115   horizontal double-wedge stimulus, spanning a polar-angle range of +/-15° around the horizontal
116   meridian, (2) a vertical double-wedge stimulus of the same kind, (3) a stimulus that covered the
117   region driven by the main-experimental stimulus (1.50°-7.04° eccentricity), (4) a 0.5°-wide ring
118   peripherally surrounding the main-experimental stimulus annulus (7.04°-7.54° eccentricity), and (5)
119   a 0.5°-wide ring inside the annulus (1.00°-1.50° eccentricity). Stimuli were presented in 6-s blocks.
120   This block length was chosen to balance temporal concentration (which increases design efficiency
121   for long blocks due to hemodynamic buildup) and stimulus adaptation (which reduces design
122   efficiency for long blocks due to reduced neuronal responses). The five dynamic stimuli and 6-s
123   fixation periods were all presented 20 times each in a random sequence over a single run lasting 12
124   min.

Subjects and task

126   *Subjects.* Eighteen healthy volunteers (13 female, age range 20-39) with normal or corrected-to-
127   normal vision took part in this fMRI experiment. Before the experiment, participants were
128   introduced to the experimental procedure and informed consent was given.

129   *Task – fMRI.* During all runs, including retinotopic mapping, subjects were instructed to continuously
130   fixate a central dot (diameter: 0.06° visual angle). Centered on the fixation dot, there was a small
131   black ring (diameter: 0.20°, line width: 0.03°), which had a tiny gap (0.03°) either on the left or right
132   side. The gap switched sides at random moments in time at an average rate of once per 3 s (with a
133   minimum inter-switch time of 1 s). The task of the subject was to continuously report the side of the
134   gap by keeping the left button pressed with the right index finger whenever the gap was on the left
135   side, and by keeping the right button pressed with the right middle finger whenever the gap was on
136   the right side. The task served to enforce fixation and to draw attention away from the stimuli.

MRI measurements and analysis

138   *MRI measurements.* Functional and anatomical MRI data were acquired with a 3T Siemens Tim-Trio
139   MRI scanner using a 32-channel head coil. During each main run, we acquired 252 volumes
140   containing 31 slices covering the occipital lobe as well as inferior parietal, inferior frontal, and
141   superior temporal regions for each subject using an EPI sequence (TR=2000 ms, TE=30 ms, flip
142   angle=77°, voxel size: 2.0 mm isotropic, field of view: 205 mm; interleaved acquisition, GRAPPA
143   acceleration factor: 2). The same EPI sequence was employed for retinotopic mapping, during which

144 we acquired 360 volumes. For each participant we also obtained a high-resolution (1 mm isotropic)
145 T1-weighted anatomical image using a Siemens MPRAGE sequence.

146 *Data preprocessing.* Functional and anatomical MRI data were preprocessed using the Brainvoyager
147 QX software package (Brain Innovation, v2.4). The first two EPI images for each run were discarded
148 (affected by T1 saturation effects). After preprocessing (slice-scan-time correction, 3D head-motion
149 correction, linear-trend removal and temporal high-pass filtering removing frequencies below 2
150 cycles per run), functional data for all subjects were aligned with the individual high-resolution
151 anatomical image and transformed into Talairach space (Talairach & Tournoux, 1988) as a step
152 toward cortex-based analysis in BrainVoyager. After automatic correction for spatial
153 inhomogeneities of the anatomical image, we created an inflated cortex reconstruction for each
154 subject. All ROIs were defined in each individual subject's cortex reconstruction and projected back
155 into voxel space. Note that we did not use Talairach space or a cortex-based common space for ROI
156 definition and within-ROI patterns were analyzed separately in each subject.

157 *Retinotopic mapping and region of interest definition*. A general linear model (GLM) was fitted to the
158 retinotopic mapping data, with five predictors for the five dynamic grating stimuli based on
159 convolving boxcar functions with the hemodynamic response function as described by Boynton et al.
160 (1996). Activation t-maps for each stimulus type were projected onto polygon-mesh reconstructions
161 of individual subjects' cortices. We determined the borders between V1-2 based on cortical t-maps
162 for responses to vertical and horizontal double-wedge stimuli Regions of interest (ROIs) were only
163 created in the portion of V1 that was more active when presenting the dynamic grating stimulus
164 covering the main-experimental annulus as compared to central and peripheral stimulation. ROIs
165 were defined as patches covering the central third portion of each quarterfield's polar range as
166 visualized in Figure 2. We excluded the remnant of the quarterfield area to reduce spillover of
167 signals between V1 quarterfield representations.

168 *Pattern-classifier analysis and orientation preference definition.* Preprocessed functional fMRI data
169 for the main experiment and individual ROI coordinates were imported into Matlab using the
170 NeuroElf Toolbox v0.9c (developed by Jochen Weber, Columbia University). With this toolbox, we
171 computed a GLM for each run of each subject, using one predictor for each stimulus type for each
172 subrun. We also included six predictors specifying 3D head motion. Each run's GLM, thus, yielded
173 four t-value activity patterns for each exemplar (one per subrun). Both runs combined yielded eight
174 t-value patterns for each exemplar. We decoded the exemplar (two orientation variants) for each
175 stimulus type with a linear support vector machine (SVM, using the libSVM library - Chang and Lin,
176 2011) using leave-two-subrun-out cross-validation (Mur et al., 2009). Cross-validation consisted of
177 four folds over which the first, second, third and fourth subrun of both runs were selected as
178 independent test data. We classified stimulus type using all voxels within the quarterfield patch ROIs
179 (gray bars Figure 3a), using only voxels with a radial or vertical preference (red bars Figure 3a) and
180 using only voxels with a tangential or horizontal preference (blue bars Figure 3a). Note that we
181 computed voxel orientation preference based only on the training data during each cross-validation
182 fold. Spurious orientation preferences (resulting from noise) will not replicate in the test data and
183 therefore cannot contribute to significant orientation decoding. Voxel orientation preference was
184 determined for each quarterfield patch by computing the mean difference of t-values between
185 orientations (e.g. radial minus tangential) taking into consideration the patch's receptive-field
186 location. For example, a voxel in a patch representing the right upper visual quarterfield was
187 considered to have a radial preference if t-values were greater for the right tilted than the left-tilted
188 grating (Figure 2). For spirals, a right-upper-field voxel would be considered to have a vertical
189 preference if t-values were greater for the counter-clockwise than for the clockwise spiral.

190 *Assessment of the effect of spatial pattern shifts on orientation decodability.* Testing data was
191 spatially shifted by 0.5, 1, 2 or 3 voxels – corresponding to 1, 2, 4 and 6 mm – using shifted ROI

192 coordinates for each patch when computing test patterns. The shift of 0.5 voxel (1 mm) was realized
193 by spatial interpolation (average of two adjacent voxels). Data was shifted in all six directions
194 (ventral, superior, left, right, anterior, and posterior). During this analysis classification performance
195 was computed as the average SVM decoding accuracy across all shift-directions within each
196 participant.

197

198

199

200 **Results**

201 ***Voxels with reliable opposite orientation preferences intermingle within small V1 patches***

202 In order to find out if V1 contains voxels with opposite orientation preferences, we considered the
203 responses to left- and right-tilted gratings in V1 patches at the center of the visual quarterfields
204 (representing polar angles 45°, 135°, 225° and 315° clockwise from vertical; Figure 2a). For a given
205 patch of voxels, each grating thus had either a radial or a tangential orientation. Contrast t maps
206 between the two gratings are shown in Figure 2a for two representative participants. These
207 unthresholded statistical maps suggest that voxels with a radial preference and voxels with a
208 tangential preference intermingle within these patches. However, opposite apparent selectivities
209 might result from the noise in the data. We therefore used decoding analyses of each of the
210 opposite-selectivity voxel sets to assess the reliability of these preferences separately.

211 First we assessed stimulus decodability using all voxels within a patch together, regardless of the
212 direction of their preference. Consistent with previous studies, decoding analyses using linear
213 support vector machines (Figure 3a) revealed that the two gratings are robustly decodable (74%
214 accuracy, p < 0.0005). The two spirals, similarly, were robustly decodable (68% accuracy, p < 0.0005;
215 Figure 3a). For the gratings, either radial- or tangential-preferring voxels, or both sets might
216 contribute to orientation decodability. For the spirals, similarly, either vertical- or horizontal-
217 preferring voxels, or both sets might contribute. Note that vertical preferences cannot contribute to
218 grating decoding, because the two gratings were balanced about the vertical orientation. Similarly,
219 radial preferences cannot contribute to spiral decoding, because the two spirals were balanced
220 about the radial orientation.

221 *Tangential- and radial-preferring voxels are intermingled and each set, by itself, supports orientation*
222 *decoding.* Single voxel responses are noisy. Even if orientation information resulted only from a
223 coarse-scale map of radial preference, we would expect some inverted preference estimates
224 (apparent tangential-preferring voxels), due to the noise in the data. In order to assess whether the
225 tangential preferences were real, we tested their reliability in the decoding framework (Figure 3a).
226 Importantly, orientation preference of voxels was determined independently from the test data.
227 Spurious orientation preferences would not replicate in the test data. We found that grating
228 orientation can be robustly decoded based only on voxels with a tangential preference (63%
229 accuracy, p < 0.0005, one-sided Wilcoxon signed-rank test across subjects). Consistent with the
230 previously reported slight bias in favor of radial preferences (Sasaki et al. 2006; Freeman et al. 2011;
231 Alink et al. 2013), decoding was also possible using only radial-preferring voxels (75% accuracy, p <
232 0.0005) and the accuracy was significantly greater for the radial-preferring voxel set than for the
233 tangential-preferring voxel set (p < 0.006, two-sided Wilcoxon signed-rank test across subjects).
234 These results show that the two opposite-preference sets of voxels, which are intermingled within
235 the patches of V1, each carry significant orientation information.

6

236 *Horizontal- and vertical-preferring voxels are intermingled and each set, by itself, supports*
237 *orientation decoding.* We performed analogous analyses on the response patterns elicited by the
238 spirals (Figure 3a). We found that spiral orientation can be robustly decoded based only on voxels
239 with a horizontal preference (56% accuracy, p < 0.04, one-sided Wilcoxon signed-rank test across
240 subjects). Again, consistent with the previously reported slight bias in favour of vertical preferences
241 (Mannion et al. 2010; Alink et al. 2013; Freeman et al. 2013), decoding was also possible using only
242 vertical-preferring voxels (68% accuracy, p < 0.0005) and the accuracy was significantly greater for
243 the vertical-preferring voxel set than for the horizontal-preferring voxel set (p < 0.02, two-sided
244 Wilcoxon signed-rank test across subjects). For the spirals, as well, results show that the two
245 opposite-preference sets of voxels, which are intermingled within small patches of V1, each carry
246 significant orientation information.

247

V1 voxels exhibit subtle radial and vertical preferences

249 In order to assess radial and vertical preferences on a group level we estimated the response
250 amplitude difference (in % signal change) between radial and tangential for all voxels across all
251 participants. We plotted the histogram of the radial-tangential response difference across V1 voxels
252 (Figure 2b – left side; pooled across quarterfield patches and the 18 participants). The histogram
253 shows that voxels in V1 are slightly more likely to prefer radial orientations over tangential
254 orientations (56.1% vs 43.9%). These proportions were significantly different (p < 0.0005, two-sided
255 across-subject t-test, test statistic: within-subject %-point difference, subject as random effect). The
256 mean response difference between radial and tangential orientations was 0.038 %-signal-change.

257 We performed analogous analyses for the spiral stimuli (Figure 2b – right side), which drive each
258 patch with either a vertical or a horizontal orientation. We plotted the histogram of the vertical-
259 horizontal response difference across V1 voxels (Figure 3b; pooled across quarterfield patches and
260 the 18 participants). The histogram shows that voxels in V1 were slightly more likely to prefer
261 vertical orientations over horizontal orientations (58.3% vs 41.7%). These proportions were
262 significantly different (p < .0005, same test as above). The mean response difference between radial
263 and tangential orientations was 0.031 %-signal-change.

264 Both the radial-over-tangential and the vertical-over-horizontal preference effect sizes were small,
265 less than 2% of the average fMRI response in these V1 patches for gratings and spirals, which were
266 2.03 %-signal-change and 2.17 %-signal-change, respectively. These results are consistent with the
267 previous analysis of this data set in Alink et al. (2013).

268

Shifting test patterns by half a voxel or more reduces orientation decodability

270 In Figure 2a, we saw that opposite orientation preferences between neighboring voxels intermingle.
271 However, voxels with similar orientation preference appear to form spatial clusters. Freeman et al.
272 (2013) recently found that the decodability of grating orientation and spiral sense is not affected by
273 shifting activation patterns by half a voxel (1 mm) between training and testing. This was taken as
274 evidence for fMRI orientation decoding relying mainly on coarse-scale orientation preference maps
275 rather than intermingled orientation preferences. To relate this finding to our data, we have
276 assessed decoding performance after shifting test patterns by 1, 2, 4 and 6 mm. Our results do show
277 strong effects of spatial shifts on decoding performance (Figure 3b). Even the minimal shift of 1 mm
278 significantly reduced decoding performance for four out of the six voxel selections (Figure 3b, p <
279 0.05). Orientation decodability for all selections was found to approach chance level for 6 mm shifts.
280 These results are consistent with the presence of information across multiple spatial scales,
281 including fine-grained and coarse-scale patterns.

282

Discussion

283

284   The aim of the current study was to find out whether fine-grained neural activation patterns
285   contribute to fMRI orientation decoding in the context of acquisition with a typical 3T scanner at a
286   spatial resolution of 2 mm isotropic. Alternatively, fMRI orientation decoding might rely solely on
287   global-areal patterns resulting from radial and vertical preferences. Previous studies used spatial-
288   frequency filtering techniques to address this question. However, spatial-frequency filtering can be
289   confounded by a high-spatial-frequency voxel gain field and can suggest the presence of fine-grained
290   pattern information where there is none (Figure 1, left). Here we exploited the fact that the voxel
291   gain field is not expected to invert the selectivity of a voxel. Therefore, reliable opposite orientation
292   selectivities within a small cluster of voxels indicate fine-grained pattern information (Figure 1,
293   right).

294   We investigated whether there are two separate sets of voxels in a small patch of V1 that have
295   opposite orientation preference. To ascertain that each set has a reliable preference (and is not just
296   inverted by noise), we performed orientation decoding on each set separately. Our main finding is
297   that grating and spiral orientation can be decoded based on voxel populations with either
298   orientation preference. This finding indicates that global-areal patterns evoked by vertical and radial
299   preference in V1 are not the only source of visual-orientation information in fMRI at 3T and supports
300   the idea that fine-grained activation patterns contribute to orientation decoding.

301   Our results are also consistent with the previously demonstrated enhanced V1 responses to radial
302   (Sasaki et al., 2006; Mannion et al., 2010; Freeman et al. 2011; Alink et al., 2013) and vertical
303   orientation (Mannion et al., 2010; Alink et al. 2013; Freeman et al., 2013) as voxels preferring
304   vertical and radial orientation were slightly more common than those preferring tangential and
305   horizontal orientation. As expected, we also found that decoding performance was greater when
306   selecting voxels preferring radial and vertical orientation for gratings and spirals, respectively. Our
307   results, thus, replicate the presence of global-areal preferences and demonstrate that fine-grained
308   patterns as well contribute to orientation decoding.

309   Recently, it has been suggested that that orientation decoding might results from differences in
310   contrast along the edges of annular gratings with different orientations (Carlson, 2014). Contrast
311   along the annular edge of a grating varies as a function of the orthogonality between the grating
312   orientation and local edge orientations. As a consequence, vertical annular gratings give rise to
313   higher contrast at the top and bottom edge while horizontal gratings lead to greater contrast at the
314   lateral edges. This edge effect is thought to give rise to global-areal activation differences similar to
315   those resulting from a radial preference. However, the edge effect does not offer a simple account
316   of spiral decoding, where edge-orientation-contrast patterns are expected to be matched between
317   stimuli (Clifford & Mannion, 2015; Carlson 2015). Therefore, edge effects might contribute a global-
318   areal component to grating decoding, but not to spiral decoding. Moreover, they do not account for
319   the local intermingling of opposite selectivities.

320   Our finding that fMRI orientation decoding is supported by fMRI voxels with opposite orientation
321   preferences does not imply that these orientation preferences have a salt-and-pepper spatial
322   distribution in V1, or that standard-resolution fMRI reflects subvoxel columnar patterns via a
323   hyperacuity mechanism (Op de Beeck et al., 2010; Kriegeskorte et al., 2010; Boynton 2005; Shmuel
324   et al, 2010). Although voxels are likely to constitute complex spatiotemporal filters (Kriegeskorte et
325   al., 2010), it is an open question whether this supports hyperacuity. Our data shows that voxels
326   preferring the same orientation tend to form clusters within V1 (Figure 2a). The fine-grained
327   orientation preferences we report might result from orientation-specific responses of veins on the
328   scale of the fMRI voxels. Veins might exhibit such a preference because their branches happen to

8

329 non-uniformly sample columns preferring different orientations. Alternatively, it has been suggested
330 that the vasculature might align itself to the functional architecture of the cortex during
331 development with veins specifically draining from columns of a particular orientation preference
332 (Gardner, 2010).

333 In summary, we demonstrate that voxels with various preferences intermingle within small voxel
334 clusters. In addition to global-areal patterns resulting from radial and vertical preferences and edge
335 effects, thus, fine-grained patterns do contribute to fMRI decoding at conventional resolution.

336

337 **References**

338 Alink A, Krugliak A, Walther A, Kriegeskorte N (2013) fMRI orientation decoding in V1 does not
339 require global maps or globally coherent orientation stimuli. Frontiers in psychology 4:493

340 Boynton GM, Engel SA, Glover GH, Heeger DJ (1996) Linear systems analysis of functional magnetic
341 resonance imaging in human V1. The journal of neuroscience 16:4207–4221.

342 Carlson TA (2014) Orientation decoding in human visual cortex: new insights from an unbiased
343 perspective. The Journal of Neuroscience 34:8373–8383.

344 Carlson TA, Wardle SG (2015) Sensible decoding. NeuroImage 110:217–218.

345 Chang C-C, Lin C-J (2011) LIBSVM: a library for support vector machines. ACM Transactions on
346 Intelligent Systems and Technology (TIST) 2:27.

347 Clifford CW, Mannion DJ (2014) Orientation decoding: Sense in spirals? NeuroImage 110:219-222

348 Freeman J, Brouwer GJ, Heeger DJ, Merriam EP (2011) Orientation decoding depends on maps, not
349 columns. The Journal of Neuroscience 31:4792–4804.

350 Freeman J, Heeger DJ, Merriam EP (2013) Coarse-Scale Biases for Spirals and Orientation in Human
351 Visual Cortex. The Journal of Neuroscience 33:19695–19703.

352 Gardner JL (2010) Is cortical vasculature functionally organized? Neuroimage 49:1953–1956.

353 Henriksson L, Nurminen L, Hyvärinen A, Vanni S (2008) Spatial frequency tuning in human
354 retinotopic visual areas. Journal of Vision 8:5.

355 Kamitani Y, Tong F (2005) Decoding the visual and subjective contents of the human brain. Nature
356 neuroscience 8:679–685.

357 Kriegeskorte N, Cusack R, Bandettini P (2010) How does an fMRI voxel sample the neuronal activity
358 pattern: compact-kernel or complex spatiotemporal filter? Neuroimage 49:1965–1976.

359 Mannion DJ, McDonald JS, Clifford CW (2010) The influence of global form on local orientation
360 anisotropies in human visual cortex. Neuroimage 52:600–605.

361 Op de Beeck H (2010) Against hyperacuity in brain reading: spatial smoothing does not hurt
362 multivariate fMRI analyses? Neuroimage 49:1943–1948.

363 Mur M, Bandettini PA, Kriegeskorte N (2009) Revealing representational content with pattern-
364 information fMRI—an introductory guide. Social cognitive and affective neuroscience:nsn044.

365 Sasaki Y, Rajimehr R, Kim BW, Ekstrom LB, Vanduffel W, Tootell RB (2006) The radial bias: a different
366 slant on visual orientation sensitivity in human and nonhuman primates. Neuron 51:661–670.

367 Shmuel A, Chaimow D, Raddatz G, Ugurbil K, Yacoub E (2010) Mechanisms underlying decoding at
368 7 T: Ocular dominance columns, broad structures, and macroscopic blood vessels in V1 convey
369 information on the stimulated eye. NeuroImage 49:1957–1964.

370 Swisher JD, Gatenby JC, Gore JC, Wolfe BA, Moon C-H, Kim S-G, Tong F (2010) Multiscale pattern
371 analysis of orientation-selective activity in the primary visual cortex. The Journal of Neuroscience
372 30:325–330.

373 Talairach J, Tournoux P (1988) Co-planar stereotaxic atlas of the human brain. 3-Dimensional
374 proportional system: an approach to cerebral imaging.

375 Yacoub E, Harel N, Uğurbil K (2008) High-field fMRI unveils orientation columns in humans.
376 Proceedings of the National Academy of Sciences 105:10607–10612.

377

378

379
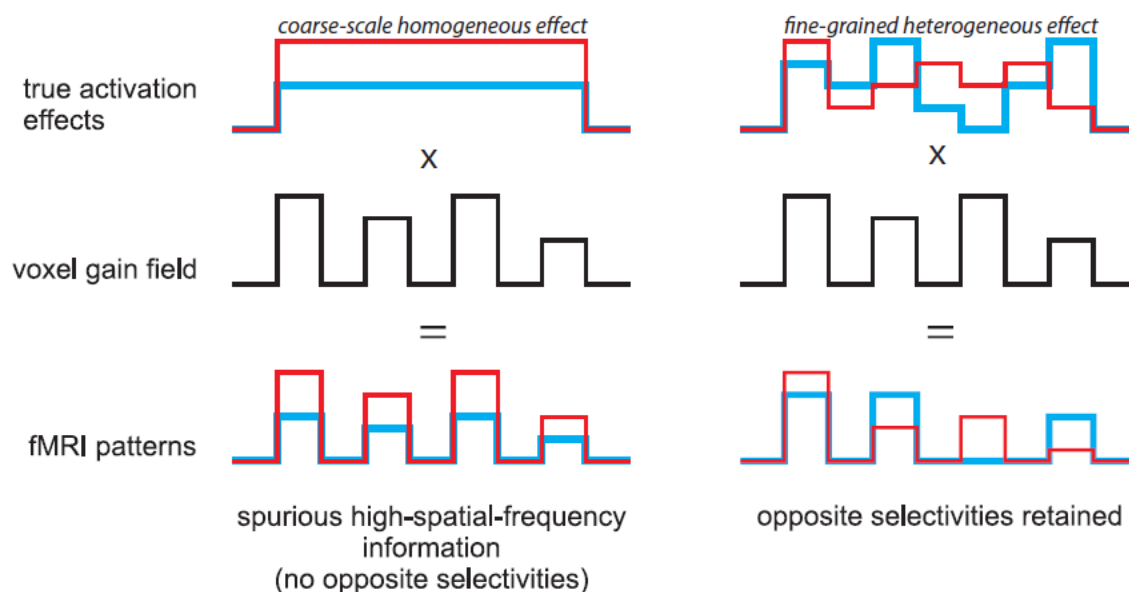
380
381
382
383 **Figure 1 – Coarse-scale neural effects can give rise to spurious high-spatial frequency fMRI pattern**
384 **information in the presence of a high-spatial frequence gain field across voxels**
385 An illustration of how differences in sensitivity to local activation across voxels (the voxel gain field)
386 can lead to spurious high-spatial- frequency information in fMRI patterns. The left column shows the
387 effect of a gain field on a coarse scale homogenous effect and the right column shows the effect of
388 gain field on a fine-grained heterogeneous effect. An important property of the gain field effect is
389 that the signs of the true activation effects are preserved. Spatial filtering analyses will suggest high-
390 spatial frequency information in either scenario (left and right). However, the signature of a fine-
391 grained heterogeneous effect (right) is the presence of local opposite selectivities (right only). Note
392 that in actual data the sign of effects can be inverted by fMRI noise; this effect is not illustrated in
393 this figure.

394

395
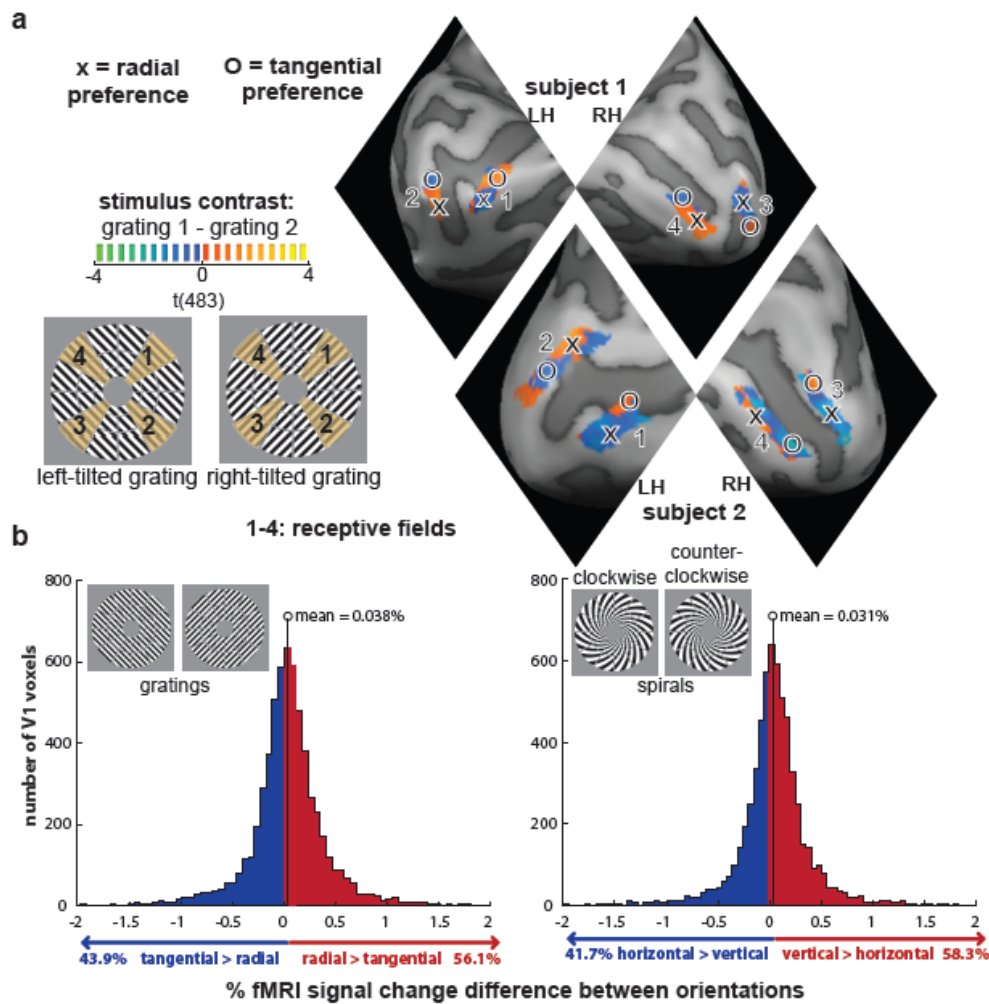
Figure 2 - opposite orientation preferences intermingle within quarterfield patches in V1

396
397   **(a)** The contrast t maps indicating the activation difference between the two displayed visual
398   gratings. Activation is only shown for the four within-quarterfield ROIs, which are labeled clockwise
399   from 1 to 4. Positive and negative t-values indicate either a radial or a tangential preference
400   depending on the visual field they are in. This we have clarified by labeling local activation clusters
401   with 0 and X when they have a tangential and radial preference respectively. Note that the
402   activation map is based on a conventional GLM t-contrast using all data. **(b)** Histograms showing the
403   distribution of V1 voxels that prefer radial vs tangential orientation (left) and vertical vs horizontal
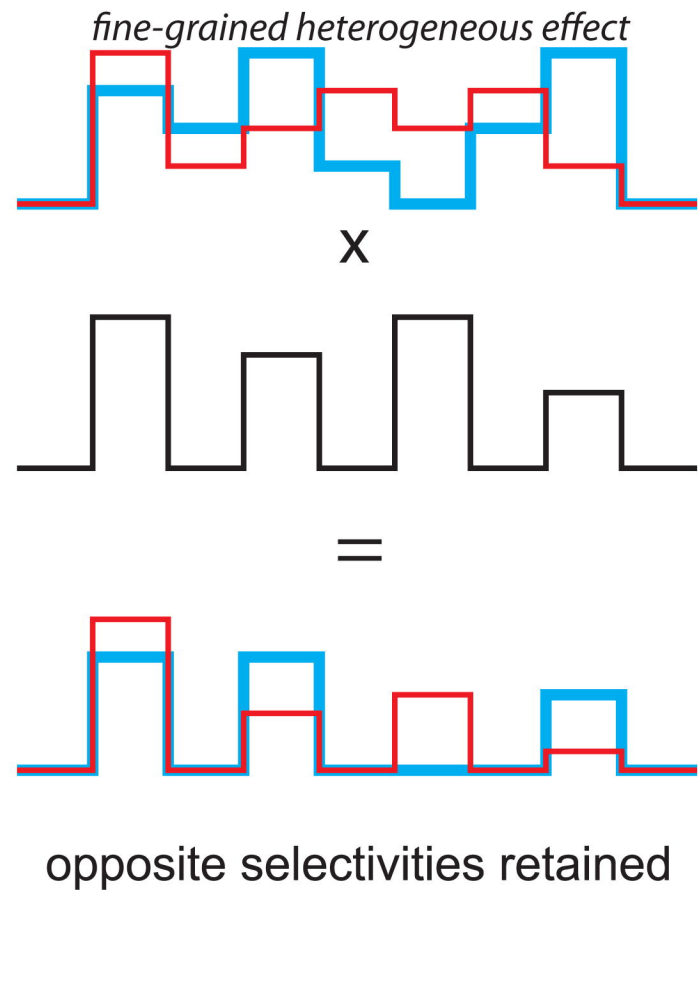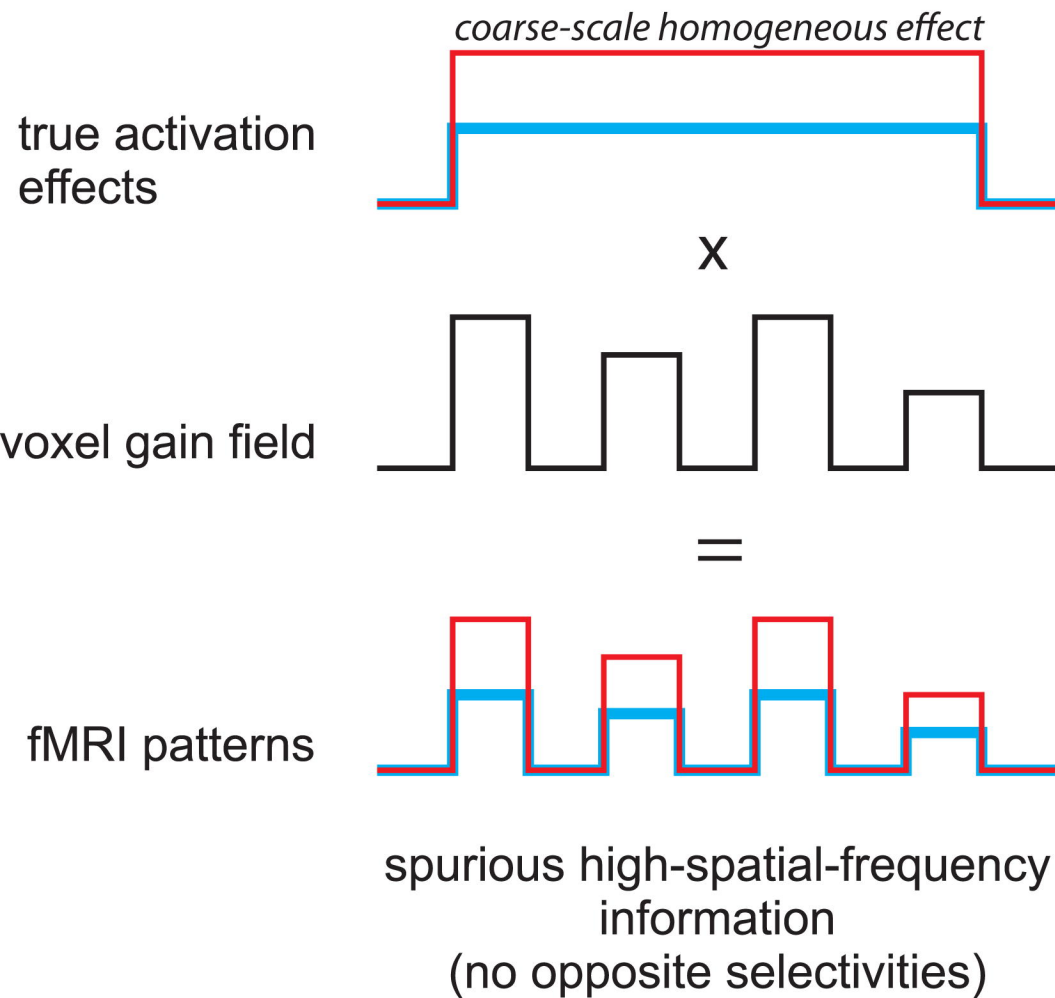404   orientation (right). These plots are based on all voxels in all ROIs across all participants.

405
406
407
408
409
410
411
412
413
414
415
416

417

418
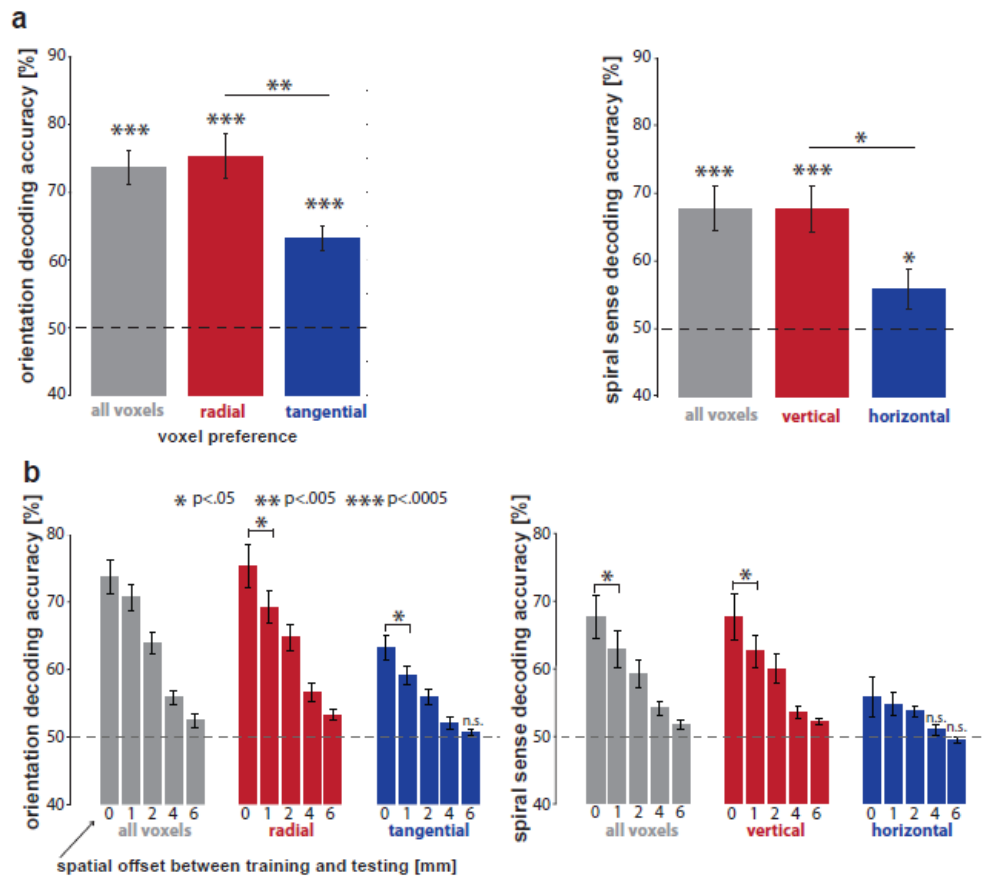
419 **Figure 3 - tangential and horizontal orientation preferences are replicable and on their own allow**
420 **for robust orientation decoding**
421 **(a)** Bar plots summarizing grating orientation (left) and spiral sense (right) decodability when
422 selecting all voxels (gray bars), voxel preferring radial/vertical preference (red bars) and voxel
423 preferring tangential/horizontal preference (blue bars). **(b)** Bar plots summarizing how grating
424 orientation (left) and spiral sense (right) decodability is affected by spatially shifting test patterns by
425 1, 2, 4 and 6 mm.
426

Acknowledgments

coarse-scale homogeneous effect

fine-grained heterogeneous effect

true activation effects

X

X

voxel gain field

=

=

fMRI patterns

spurious high-spatial-frequency information
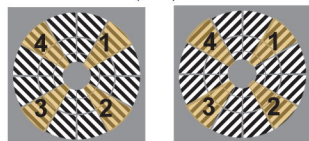(no opposite selectivities)

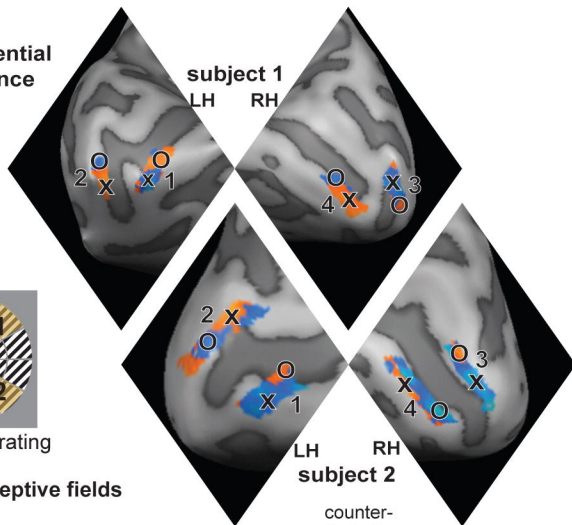opposite selectivities retained

a

x = radial preference   O = tangential preference

stimulus contrast:
grating 1 - grating 2

t(483)   -4 ··· 0 ··· 4

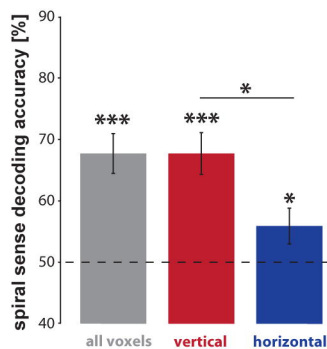left-tilted grating   right-tilted grating

subject 1
LH   RH

subject 2
LH   RH

1-4: receptive fields

b

mean = 0.038%

gratings

number of V1 voxels

-2 -1.5 -1 -0.5 0 0.5 1 1.5 2

43.9% tangential > radial   radial > tangential 56.1%

clockwise   counter-clockwise

mean = 0.031%

spirals

-2 -1.5 -1 -0.5 0 0.5 1 1.5 2

41.7% horizontal > vertical   vertical > horizontal 58.3%
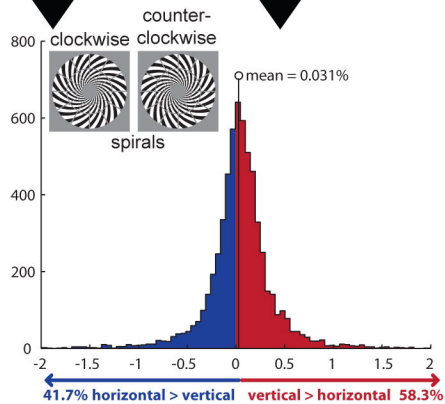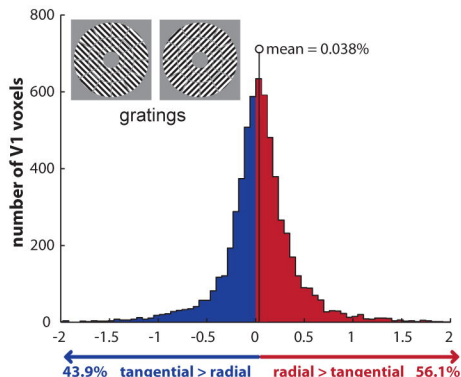
% fMRI signal change difference between orientations